IOP Publishing Physica Scripta
Phys. Scr. **95** (2020) 035602 (10pp) https://doi.org/10.1088/1402-4896/ab4bae

Characterization of argon plasma in a variable multi-pole line cusp magnetic field configuration

A D Patel, M Sharma, N Ramasubramanian, J Ghosh and P K Chattopadhyay

Institute for Plasma Research, HBNI, Bhat, Gandhinagar, Gujarat—382428, India

E-mail: amitphy9898@gmail.com

Received 7 April 2019, revised 6 August 2019
Accepted for publication 7 October 2019
Published 3 February 2020

Abstract

This paper presents a detail characterization of argon plasma confined by a multi-pole line cusp magnetic field (MMF) over a large cylindrical volume (1 m axial length and 40 cm diameter) (Patel *et al* 2018 *Rev. Sci. Instrum.* **89** 043510) and various magnetic field scaling with magnet current obtained from the magnetic field simulation in the vacuum. From the experimental results, it has been observed that in this field configuration the confinement of the primary electrons increases and leak width (plasma escaping through the cusp) of plasma decreases with increasing the magnetic field. As a result the mean density, particle confinement time and the stability of the plasma increase with increasing magnetic field values. In addition to this, it has been also observed that the radial uniformity of the plasma density across the magnetic field explicitly depends on the magnetic field values of MMF. Moreover, the nature of turbulence in a quiescent argon plasma has been identified.

Keywords: multi-pole line-cusp, electromagnet, plasma source

(Some figures may appear in colour only in the online journal)

1. Introduction

The multi-pole cusp magnetic field (MMF) confines a large volume of high-density uniform and quiescent plasma [1, 2]. Due to these abilities, it has found a wide application in the development of ion sources which include plasma etching reactors [3], ion implantation [4], deposition [5, 6] and NBI system for nuclear fusion devices [7–9]. MMF is usually created by placing rows of magnets along the length of cylindrical plasma chamber with alternating polarity. In 1973, Limpaecher and MacKenzie first observed that MMF generated by permanent magnets can increase the density of a DC discharge plasma [1]. Later confinement of plasma in different cusp geometries has been investigated in 1975, and it was observed that a full-line cusp geometry gives the highest density by confining primary electrons [9]. In general, there are three important parameters associated with MMF design for plasma sources; firstly, the area of field free region, secondly line cusp loss width of plasma and lastly control over the radial uniformity across the magnetic field. Here the field-free central region plays a crucial role in producing a well collimated ion beam source as it determines the volume available for the formation of uniform plasma. Also, for proper emission of electrons from the filaments to generate a uniformly dense plasma, the filament should be kept at the field free region. The area of the field-free region of MMF is usually adjusted by varying of a number of the pole magnets [8]. The second crucial confinement property involved with the cusp magnetic field is the effective plasma leak width i.e. the width of the profile of plasma escaping through the cusp [10, 11]. The cusp loss width governs the efficiency of plasma source [10, 11]. An exact scaling for the amount of plasma leaking is not known yet explicitly, though many scales ranging from ion gyro-radius to electron gyro-radius have been published in the literature [10–19]. The last crucial confinement property of MMF based plasma sources is radial uniformity of plasma density across the magnetic field. Earlier research in cusp magnetic field geometry the radial uniformity

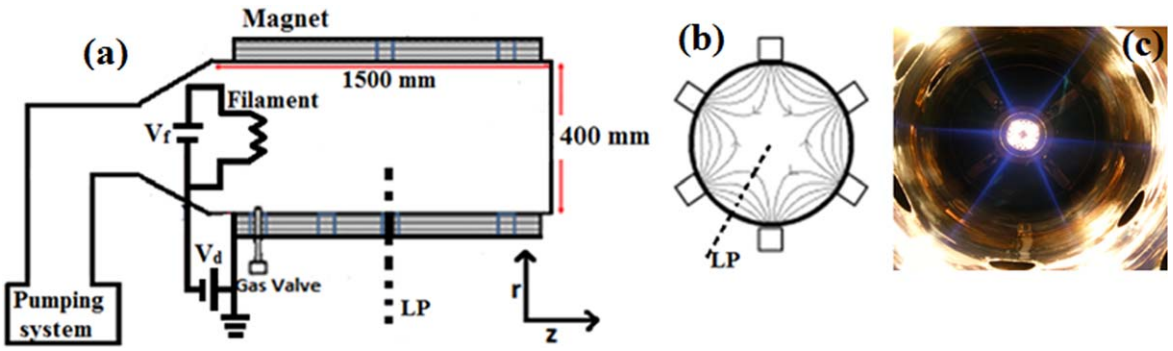

Figure 1. Schematic diagram of (a) experimental setup and (b) chamber end cross sectional view of the multi-pole line cusp magnetic field plasma device, where LP-Langmuir probe, V_{fil}-floating power supply for filament heating, V_d-discharge power supply. (c) An image of the argon plasma taken from the viewport fitted at the end of the chamber.

can be changed with changing permanent magnets [9, 20]. These devices do not have control over the area of null region of cusp magnetic field and hence on the mean plasma density, radial uniformity of plasma density unless the number of poles are changed.

In this present article, we have demonstrated a detailed characterization of argon plasma in a multi-pole line cusp magnetic field with varying magnetic field values. The MMF has been produced by placing six electromagnets (with embedded profiled vacoflux-50 core, It is a Soft magnetic alloy of iron and cobalt in the ratio 50:50 with low coercive field strength) over a large volume (1 m axial length and 40 cm diameter). The edge of vacoflux-50 core material is profiled to avoid edge effect on magnetic field lines. Similar field lines have been observed by performing simulation using field element method magnetics (FEMM) tools [21]. The MMF has control over the size of the null region without changing the number of the poles. Also, the rate of change of pole magnetic field (maximum magnetic field) with respect to magnet current for vacoflux-50 core electromagnet is too high compared to simple air core electromagnets. The argon plasma has been produced by a hot cathode filament based source located at the center of one end of the chamber. The argon plasma has been characterized for different values of a magnetic field of a MMF and the results show that MMF has control over mean plasma density, radial uniformity of plasma density and confinement of primary electrons. The rest of the paper is arranged as follows: section 2 describes the brief description of the experimental setup. section 3 described the profiling of magnetic field lines using profiled vacolfux-50 as a core material and comparison of the simulation results for magnetic field values by changing core material i.e. air core and vacoflux-50 core. Section 4 describes the experimental observation and results on confinement of primary electron and leak width of plasma and its effect on plasma parameters by changing magnetic field values of MMF. In addition the turbulence in a quiescent argon plasma will be discussed in this section. Finally in last section we conclude the article.

2. Experimental setup

The experimental setup consists of a cylindrical vacuum chamber (diameter = 40 cm and length = 1.5 m) as shown in figure 1(a). Figure 1(b) shows its cross sectional view of device and figure 1(c) shows an image of the argon plasma taken from the view port fitted at the end of the chamber. This chamber is pumped out by a combination of Rotary-Turbo Molecular Pump (430 l s^{-1}) pump capable of 10^{-6} mbar base pressure. The cusp magnetic field has been produced by six rectangular electromagnets and magnetic field is profiled using vacoflux-50 core material. The filamentary argon discharge plasma is produced using hot filament based cathode source. The plasma source (cathode) is two dimensional (8 cm × 8 cm) vertical arrays of five tungsten filaments; each filament has 0.5 mm diameter and 8 cm length. It is fitted from the conical reducer such that the filaments are inside the main chamber itself where the magnetic field is low. Also it has been taken care to push the source well inside the main chamber to avoid the edge effects of the magnets. These filaments are powered in parallel by a 500 A, 15 V floating power supply (V_{fil}) while it is normally operated at around 16–19 A per filament. The chamber was filled with rgon gas through a needle valve to a pressure 2×10^{-4} mbar. The filament is biased with a voltage of −76 V with respect to the grounded chamber walls using discharge power supply (V_d). The primary electrons emitted from the filaments travel in the electrical field directions towards chamber wall anode, while they are confined by the cusp magnetic field lines. All experimental measurements as well as the radial profile of plasma parameters are measured along the non-cusp region (the region in between two consecutive magnets) are carried out at mid (r, θ) plane of the device which is $z = 65$ cm away from the filaments at 2×10^{-4} mbar until and unless specified [22].

3. A versatile multi-pole line cusp magnetic field (MMF)

Initially, a finite element method magnetics (FEMM) [21] simulation is performed for MMF assuming permanent

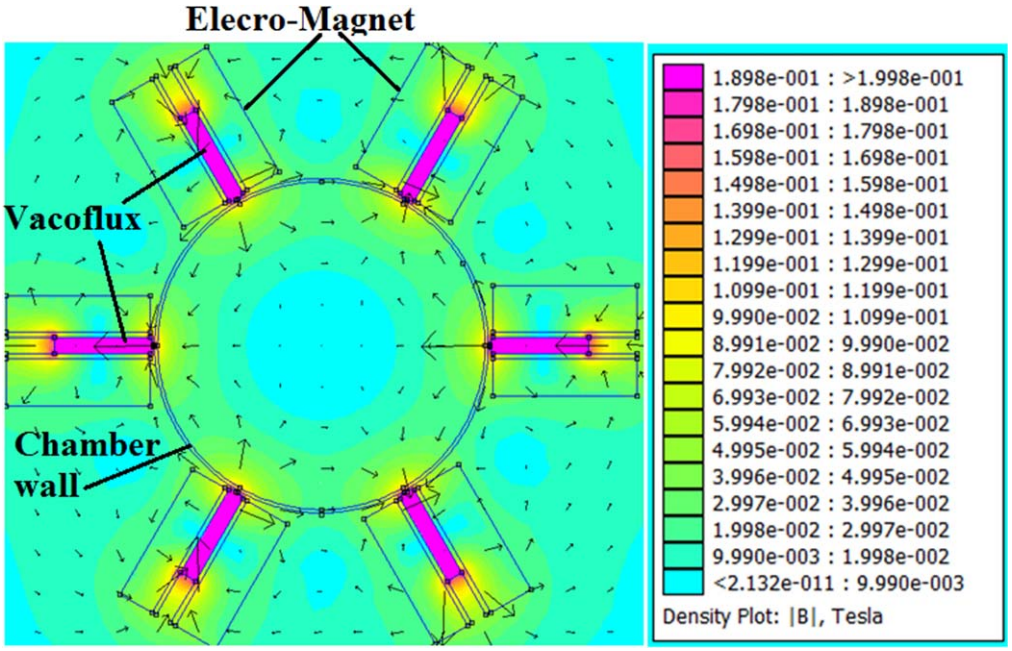

Figure 2. Contour plot of the vacuum field lines in (r, θ) mid plane of device from FEMM simulation when core is magnetized with 150 A, magnet current. Arrows shows magnetic field direction.

magnets to finalize the size and axial length of the chamber to satisfy the basic experimental requirements. After a lot of iteration using FEMM simulation, we have found that the cusp magnetic field using six permanent magnets having the length of 1 m kept in the multi-pole cusp configuration at 60° each along the circumference of a 40 cm diameter cylinder full fill all the requirements of our physics studies. However to realize variable field free zone, variable cusp magnetic field geometry is necessary which can fulfilled by same number of electromagnets with profiled core material. Each electromagnet is made with double pan-cake windings using hollow copper pipes. The hollow copper pipes are used for forced water cooling and the pan-cake windings help for effective cooling using parallel lines. The physical dimensions of the rectangular magnet are in centimeter 132, 19.5 and 14 respectively for length, width, and height. Similarly the physical dimensions of vacoflux-50 core material dimensions are in centimeter 120, 2 and 12 respectively for length, width and height [22]. This core material is an alloy of iron and cobalt in the ratio 50:50. The physical property of core material i.e. relative permeability (>4000), saturation flux density (>2.0 Tesla) and Curie temperature (700 °C) of Vacolfux-50 are too high and these properties are increased strength of MMF.

To understand the scaling of magnetic field with respect to the magnet current, FEMM simulation has been carried out at different magnet currents. The model for VMMF is constructed in FEMM tool, and the simulations are performed for air and for vacoflux-50 core (simply change the property of core material in the model) with core is magnetized by changing magnet currents (I_{mag}). The simulations are also performed with changing the shape of the edge surface of core in the model for showing the effect of core edge surface on magnetic field lines. The results obtained from the magnetic field simulations are described as follow.

Figure 2 shows the contour plot of the vacuum field lines in (r, θ) plane of the device from FEMM simulation when core material is magnetized with 150 A magnets current. It shows six electromagnets with embedded vacoflux-50 core are placed over a periphery of 40 cm diameter of the chamber. The magnetic field is measured over the different (r, θ) plane of the device using triple axis gauss probe (F W Bell, model Z0A99-3202) and suitable gauss meter (F W Bell series 9900). The measured magnetic field is good matched with simulation magnetic field as shown in figure 4 in our earlier article [22]. Figure 3 shows contour plot of the vacuum field lines of an electromagnet with air as a core (figure 3(a)) and vacoflux-50 as a core (figure 3(b)) when core is magnetized with 150 A magnet current. For an air core magnet, magnetic field lines pass through whole magnet. However, for the vacoflux-50, magnetic field lines pass through only the core, resulting dense magnetic field lines at the pole for vacoflux-50 core. Thus magnetic field is higher for vacoflux-50 core at the pole as compared to the air core. The edge of core material which affects the magnetic field lines has been also taken care. The sharp edge of core material distorts the magnetic field lines which cause the non-uniform distribution of field lines near the surface of the core. This sharp edge effect of core material on magnetic field lines is overcome by making curved edge of core material as shown in figure 4(a). It shows the cross-sectional view of the vacoflux-50 material, the edge of vacoflux-50, which is profiled in curved shape with a radius of curvature of 12.32 mm. Figure 4(b) shows FEMM simulation of magnetic field lines at core edge is curved and figure 4(c) shows the edge of the core make sharp (rectangular). It is clearly visible from figure 4(b) that magnetic field

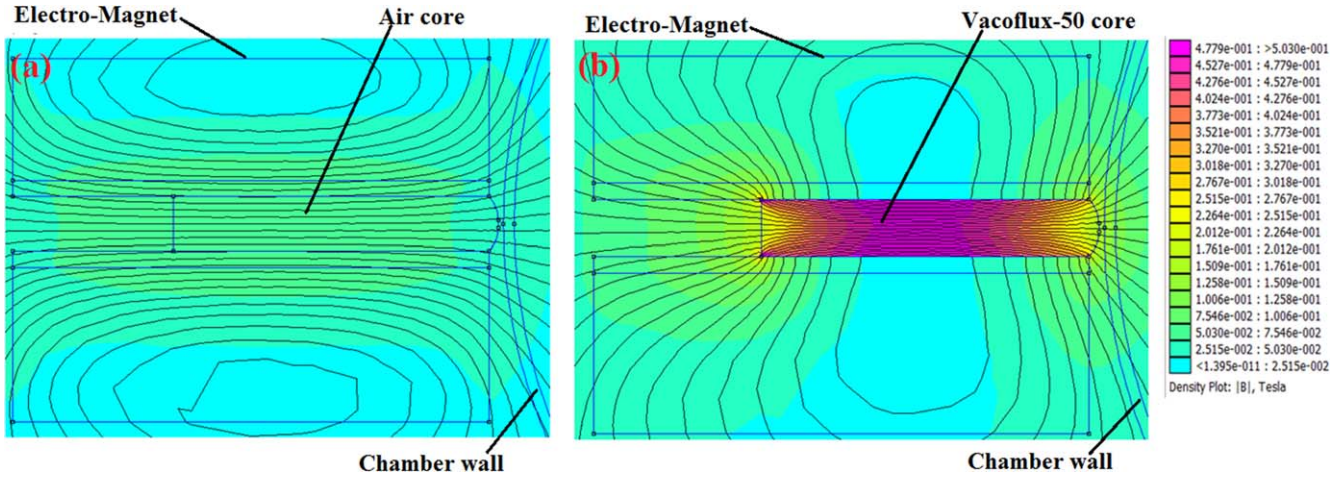

Figure 3. Contour plot of the vacuum field lines of electromagnet (a) for air core (b) for vacoflux-50 core when core is magnetized with magnet current 150 A using FEMM simulation. Solid lines shows the magnetic field line.

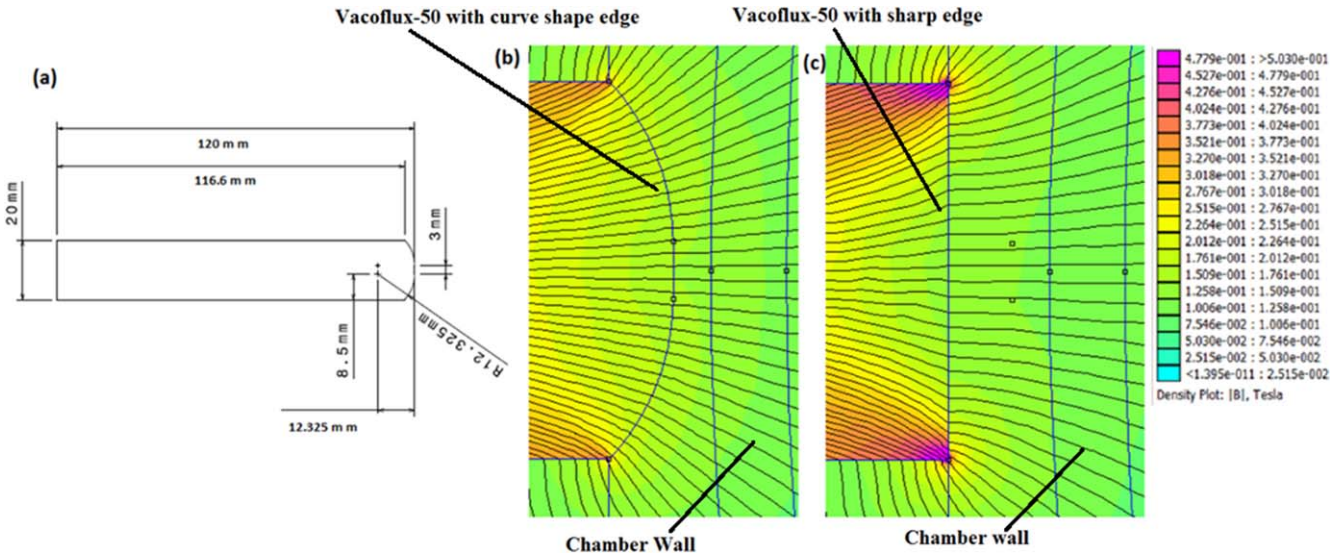

Figure 4. (a) Cross sectional view of vacoflux-50 showing curvature surface at one edge. Other two figure shows FEMM simulation of field lines for (b) edge of vacoflux-50 is curved and for (c) edge of vacoflux-50 is sharp (rectangular) when core is magnetized with 150 A magnet current (I_{mag}). Solid line shows the field line.

lines are uniformly distributed over the curved edge vacoflux-50 core.

Figure 5(a) shows the radial variation of magnetic field and figure 5(b) shows its gradient along the cusp region as well as along the non-cusp region for air core and for vacoflux-50 core, when the core is magnetized with magnet current (I_{mag}) 150 A. It can be clearly observed from both the figures that in the nearly field free region, the gradient is weak and nearly equal for both core. Beside near the pole (near the edge of the device), the gradient in the magnetic field increases sharply for vacoflux-50 core compared to air core along the cusp region. Figure 5(c) shows the variation of pole magnetic field (B_p, near the magnet at $R = 20$ cm) with respect to magnet current for air core and vacoflux-50 core. The rate of change of pole magnetic field (B_p) with respect to magnet current is very high (7.53 G A^{-1}) for vacoflux-50 core compare to air core (2.15 G A^{-1}). Figure 5(d) shows the radial variation of the magnetic field in the cusp region when magnets are energized with different currents. It can be clearly observed that the radius of nearly field free region is decreased with increasing magnet current. Thus, using electromagnets with the core material, field values can be varied by varying magnet current with the effect of using different permanent magnets and the volume of nearly field free region (null region) also changed with changing magnets current without changing the number of the poles.

4. Experimental results and discussion

The MATLAB code is developed using technique used by Sheehan *et al* [23], for analysis the *V–I* characteristic of plasma. A detailed analysis of electron temperature (T_e) has been reported in our earlier publication [22]. In our experiments, the Debye number (ratio of the probe radius to the Debye length) vary from 3 to 10. The plasma density (n) is

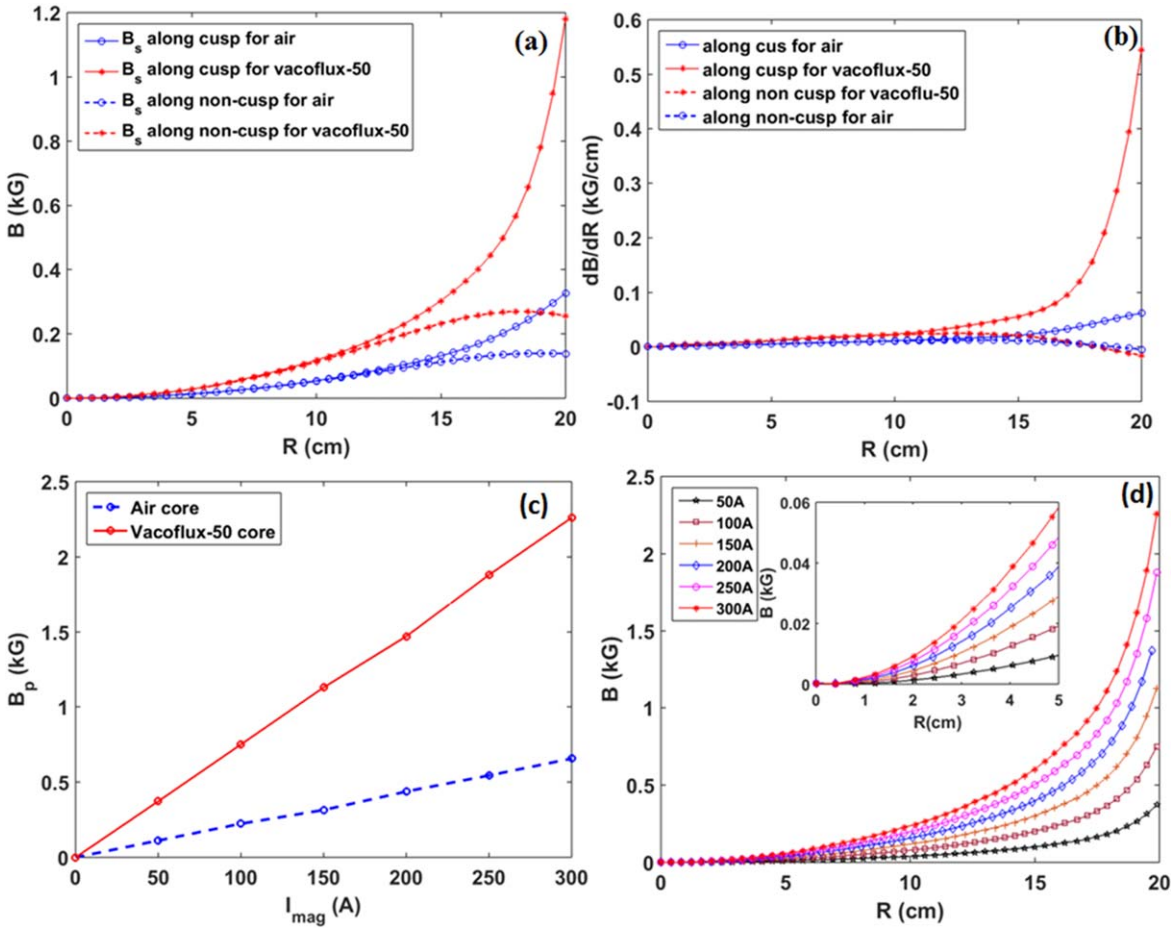

Figure 5. (a) Radial variation of magnetic field along cusp region and non-cusp region, (b) its gradient with respect to radial distance for vacoflux-50 and air core and magnet current (I_{mag}) is 150 A. (c) Variation of pole magnetic field (B_p) (at $R = 20$ cm, near the pole of magnet) with magnet current for air core and vacoflux-50 core. (d) The radial variation of magnetic field along the cusp region whenvacoflux-50 core is magnetized with different currents (I_{mag}).

determined from the ion saturation current by assuming the plasma to be quasi-neutral ($n_e \approx n_i = n$). The details of density (n) determination are given in [22] and [24]. The values of T_e and n give us the information of cusp characteristics in term of leak width. We now describe the experimental results on confinement property of MMF i.e. leak width of plasma and its effect on confinement of primary electrons, plasma density, particle confinement time, and density fluctuation with changing magnetic field and letter we describe turbulence in quiescent argon plasma confined by a variable cusp magnetic field.

4.1. Leak width

The plasma confined in multi pole line cusp magnetic field, follows the cusp field lines and streams radially outward. While following the field lines plasma losses to the boundary of the device to the narrow regions where the magnetic field lines intersect the wall, known as loss area or leak width as shown in the figure 6. The leak width (d) of quasi-neutral plasma flowing out of a cusp and cross field diffusion is

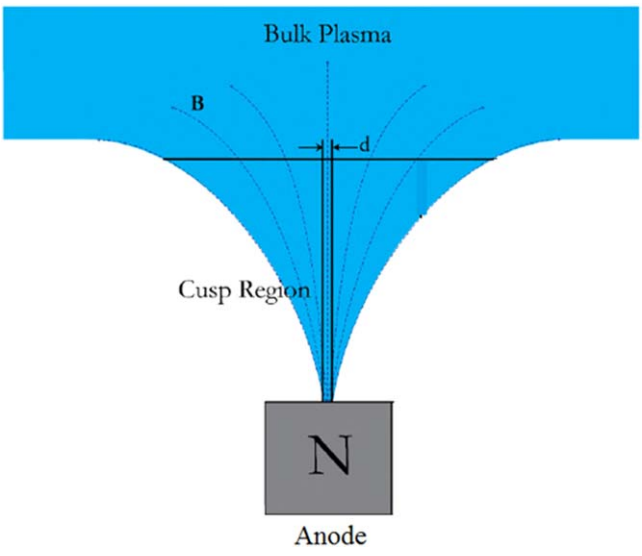

Figure 6. Schematic representation of leak width at the cusp region.

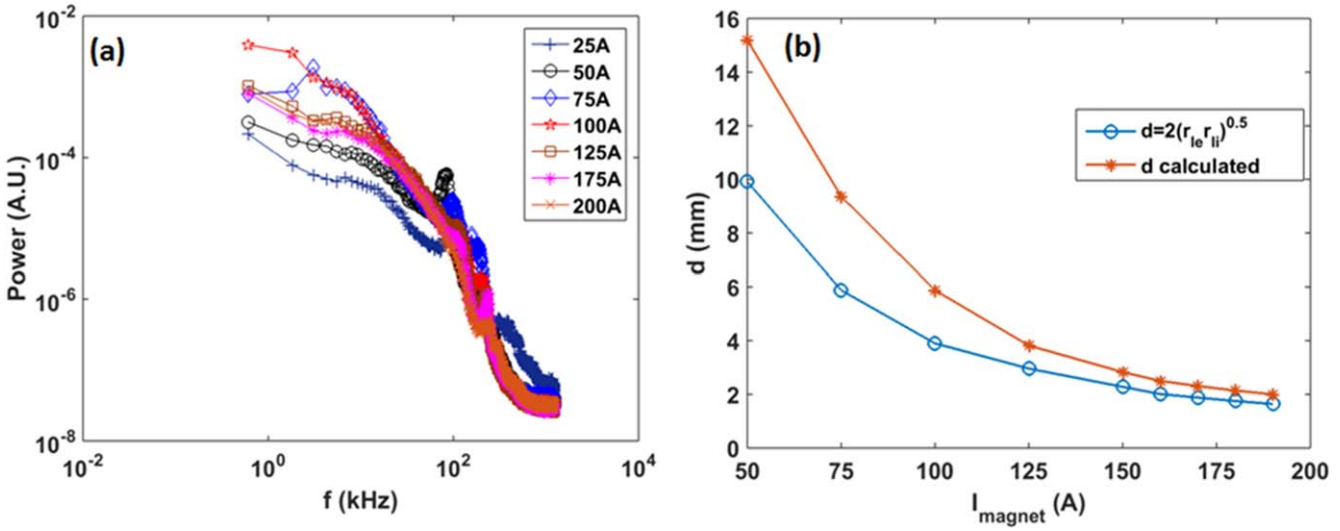

Figure 7. (a) Density autopower spectra at $R = 16$ cm in cusp region near the pole and (b) comparision of leak width between calculated from equation (2) and calculated from hybrid gyro radius at $R = 16$ cm in cusp region when core is magnetized with different current.

dominated by Bohm diffusion is given by [10, 11]

$$d = \left(\frac{D_\perp L}{C_s}\right), \tag{1}$$

where, $D_\perp$ is diffusion coefficient across the magnetic field near the pole of magnet, L is scale length of magnetic field (B) and c_s is the ion acoustic speed.

In low background gas pressure, Jones (1981) relates the leak width (d) to plasma turbulence [15]. Micro-instabilities which are unstable in a cusp sheath (e.g. drift wave, ion cyclotron waves) give rise to Bohm like diffusion [15, 16]. The relationship between the relative electron density fluctuation level $\delta n_e/n_e$ and the leak width (d) for turbulent line cusp [16]

$$d \geqslant \frac{\delta n_e}{n_e}\frac{T_e}{T_i} r_{\mathrm{Li}}, \tag{2}$$

where n_e the electron density is r_{Li} is ion larmor radius, T_e and T_i are electron and ion temperature respectively.

The density fluctuation have been measured at $R = 16$ cm near the pole in cusp region. The power spectra of density fluctuation at different magnet current are shown in figure 7(a). The observed turbulence have broad band spectra with significant power. Hence considering turbulant line cusp, we use equation (2) for leak width calculation. In equation (2), we consider $\frac{\delta n_e}{n_e} \approx \frac{\delta I_{\mathrm{esat}}}{I_{\mathrm{esat}}}$ where I_{esat}, the electron saturation current is observed in the cusp region at $R = 16$ cm and it is also considered that the ion temperature (T_i) is 10 times less than the electron temperature (T_e) [25]. The electron temperatures (T_e) and electron saturation currents (I_{esat}) are measured from same single Langmuir probe at $R = 16$ cm near the pole of magnet. The leak width (d) from equation (2) at different magnetic field values are calculated and plotted as shown in figure 7(b). For comparison, the leak widths calculated from hybrid gyro-radii $d = 2(r_i r_e)^{0.5}$ [25] are also plotted in the same figure 7(b). The leak width of plasma decreased with the increase of current in the magnets and hence decreasing the loss rate of bulk plasma through the cusp. The leak widths from both expressions are found to be matching well at high magnetic field values but the values are found to be different for low magnetic field values and these results are consistent with results obtained by Bosh *et al* [10, 11]. The leak width of plasma is decreased with increasing magnet current and hence decreasing the loss rate of bulk plasma. Thus it effect the plasma parameters i.e. plasma density, floating potential, and particle confinement time.

Now, we describe the effect of leak width on plasma parameters as well as on the radial variation of plasma parameters. Figure 8 shows the variation of floating potential at $R = 0$ cm with magnets current (I_{mag}). The leak width of plasma is decreased with increasing magnet current as shown in figure 7(b) because of that leak rate of plasma decreased hence confinment of primary electron increased. Thus, the floating potential becomes more and more negative with increasing the magnet current as shwon in figure 8. This can also be verified by measuring the primary electron density. Leung *et al* [12], had defined the primary electron density by the equation

$$n_p = -\left(\frac{2m_e v_p}{e^2 A_p}\right) \mathrm{d}I/\mathrm{d}V. \tag{3}$$

where, m_e is electron mass, $v_p = \sqrt{2eV_d/m_e}$ is primary electron velocity, V_d is discharge voltage, A_p is probe area and $\mathrm{d}I/\mathrm{d}V$ is slope of tail part of the maxwellian distribution of I–V characteristic. Figure 9 shows the variation of typical I–V characteristic of plasma after subtracting the ion saturation current at the center of device with different current in the magnets. It is observed from the figure 9 that the slope $\mathrm{d}I/\mathrm{d}V$ increases with the increasing pole magnetic field values. This shows that the primary electron density increases with the increasing magnetic field values. These confined primary electrons make more collision with neutral background argon gas atoms and enhance the plasma density as well as leak rate

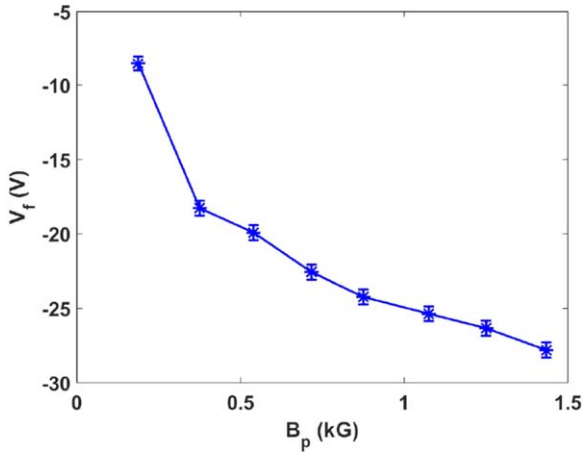

Figure 8. Variation of floating potential (V_f) at the center of the device ($R = 0$ cm) with pole magnetic field (B_p) by changing current in the magnets and 2×10^{-4} mbar argon gas pressure.

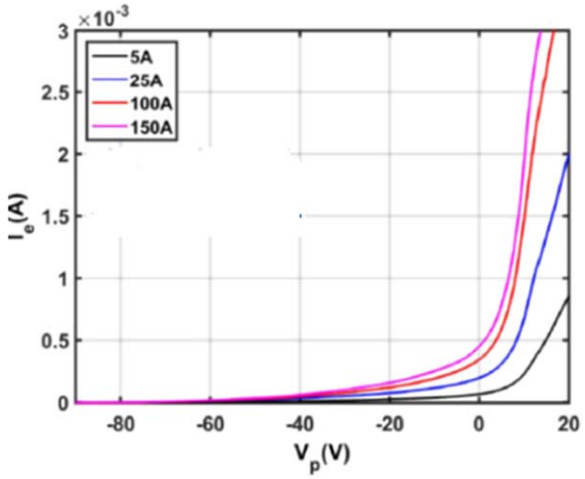

Figure 9. Variation of *I–V* characteristics of plasma after subtracting ion saturation current with changing current in the magnets at the center of the device ($R = 0$ cm) and 2×10^{-4} mbar argon gas pressure.

of plasma also decreased with increasing magnet current (magnetic field) thus the plasma density in confined region (near $R = 0$ cm) is increased with increasing magnet current as shown in figure 10(a) [22].

Figure 11 shows the radial variation of floating potential across the magnetic field along the non-cusp region. The cusp magnetic field confined the primary electrons in confined region (null region) and scavenged these electron across the magnetic field thus floating potential is highly negative at confined region and decreased radially outwards across the magnetic field. The floating potential of confined region also become more and more negative with increasing magnet current because confinement of primary electrons is increased with increasing magnet current. The scavenging radial length across the magnetic field (i.e. floating potential become nearly −5 V at radial distance 7 cm, 6 cm, and 5 cm for 100 A, 150 A, and 200 A magnet current respectively) decreased with increasing magnet current. Thus MMF scavenged the primary electrons across the magnetic field and act as like

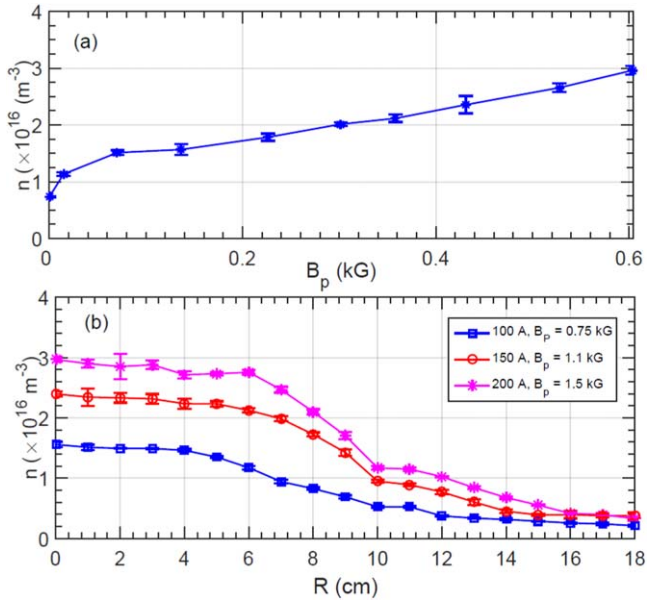

Figure 10. (a) Variation of plasma density (n) with change in magnet current at $R = 0$ cm, center of the device, (b) radial variation of plasma density along the non-cusp region for 100, 150 and 200 A, for 2×10^{-4} mbar argon gas pressure; B_p is the pole magnetic field value at $R = 20$ cm [22].

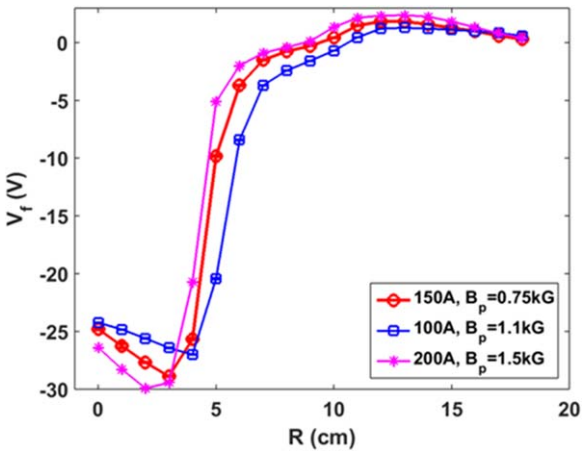

Figure 11. The radial variation of mean floating potential across the magnetic field and along non-cusp region, when core is magnetized with three different magnet currents.

filter, and it has also control over filtering strength (scavenging length). The confined primary electron at confined region move back and forth between two poles and make collision with background gas atoms, the collision may ionize or excite the argon gas atom. In figure 1(c), the deep purple colors are first excitation energy of argon atom and it take place only when the temperature of the electron is more than 3 eV thus deep purple color shows the path of primary electrons.

The radial uniformity of plasma density across the magnetic field along the non-cusp region as shown in figure 10(b) in is 4 cm, 5 cm and 6 cm for 100 A, 150 A and 200 A magnet current respectively [22]. As we increase the magnetic field the leak width of plasma decreases thus

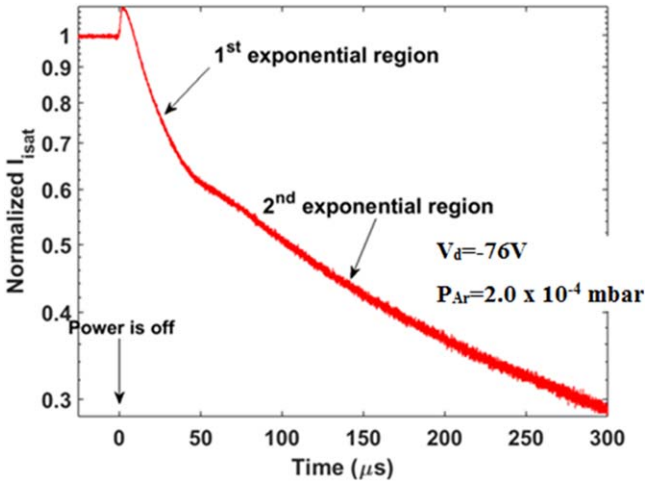

Figure 12. Time profile of normalized ion saturation current in the afterglow plasma at the center of the device when current in the magnets (I_{mag}) is 150 A, and 2×10^{-4} mbar argon gas pressure.

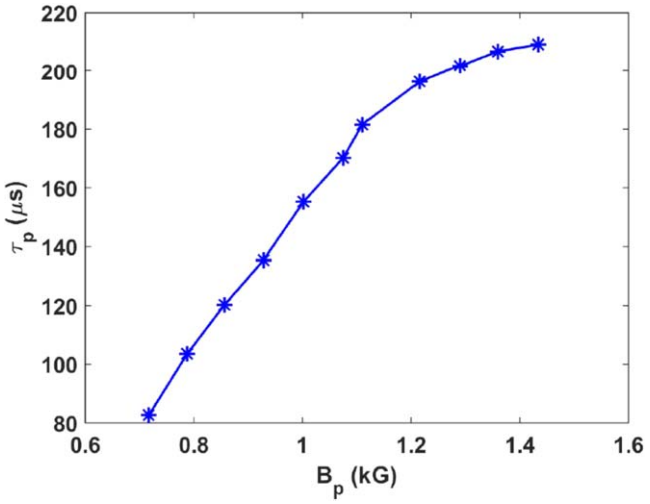

Figure 13. Variation of particle confinement time with pole magnetic field (B_p) by changing current in the magnets and 2×10^{-4} mbar argon gas pressure.

parallel diffusion lose rate decreased. Beside plasma density increases with decreasing leak width thus plasma species make more collisions with each other. As a result perpendicular diffusion coefficient increases and hence radial plasma density uniformity are increased with magnetic field (magnet current).

The confinement of the plasma needed more insight through particle confinement time for different field values. The particle confinement time can be estimated from the time profile of ion saturation current in an afterglow plasma. The afterglow plasma is usually created and studied by switching off the filament discharge power. Repetitive afterglow plasmas can be created by using a possible switching ON/OFF mechanism in discharge circuit. The discharge power supply is switched OFF and ON for 500 ms and the dc ion saturation current across the 10 kΩ resistance is recorded simultaneously. Figure 12 shows the typical time profile of normalized ion saturation current (I_{isat}) in an afterglow plasma, when probe is located at $R = 0$ cm and pole magnetic field is 1.1 kG. The time taken by ion saturation current to reduce $1/e$ of its initial value is defined here the particle confinement time. From figure 12, it can be observed that the time profile of ion saturation current has two exponential regions representing the plasma to be associated with two particle confinement times. As the cusp magnetic field confines primary electrons, after switching off the discharge power supply, the confined energetic (primary) electron move back and forth along the field lines and ionize the background gas. First rapid exponential is due to plasma bulk electron and second exponential is due to the energetic trapped electrons in cusp magnetic field [26]. Figure 13 shows the variation of particle confinement time with changing current in the magnets. Since the leak width of plasma is decreased with the increasing magnet current (or magnetic field), because of that plasma density at the confined region is increased and a leak rate of plasma is decreased, thus particle confinement time increases with magnet current (or magnetic field) as shown in figure 13. The stability of plasma also increased with increasing the

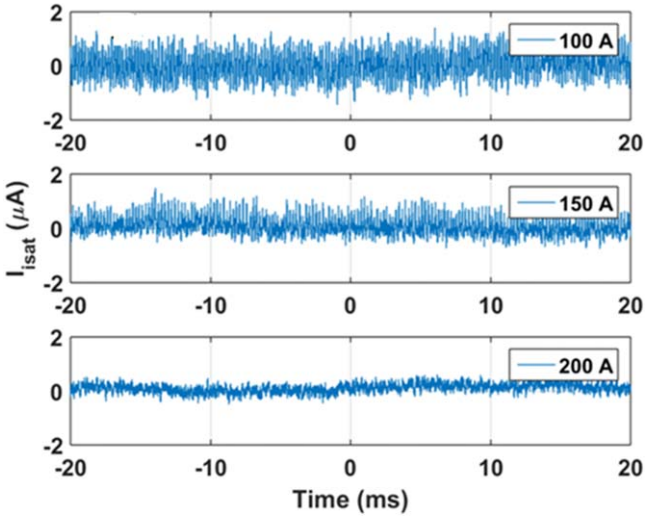

Figure 14. Time profile of ion saturation current fluctuations at $R = 0$ cm when core material is magnetized with different magnet current (I_{mag}).

particle confinement time and plasma density. The increase in plasma stability also seen from figure 14 that fluctuation in ion saturation current (density) at $R = 0$ cm is decreased with increasing magnet current.

4.2. Turbulance in quiscent argon plasma

In this section we describe the turbulence at quiescent plasma ($\delta n/n \sim 1\%$) confined in the null region of the device. The important characteristic features such as comparison of fluctuation in plasma parameters, auto-power spectra, cross correlation function are necessary to investigate and identify the instability or turbulence. The cross correlation function between the normalized values of density fluctuation ($\delta n/n$) with floating potential fluctuation (eV_f/k_BT_e) is found to be strongly correlated as shown in figure 15. The correlation coefficient obtained is nearly $c(\tau) \sim 0.8$. These

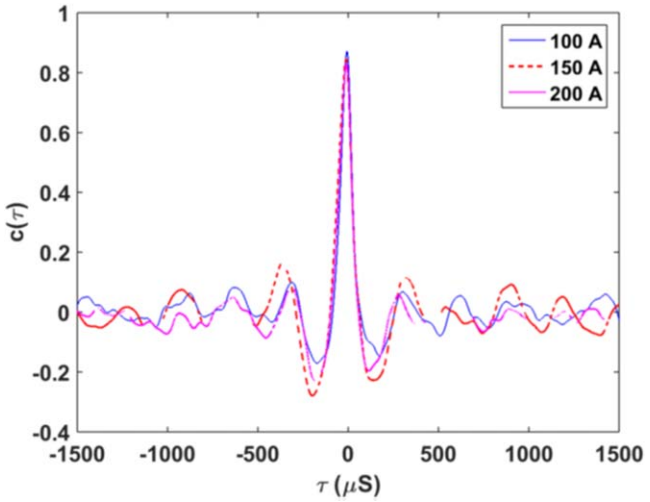

Figure 15. The cross correlation function $c\ (\tau)$ between normalized time series of density and floating potential fluctuation at $R = 0$ cm when core material is magnetized with different magnet current (I_{mag}).

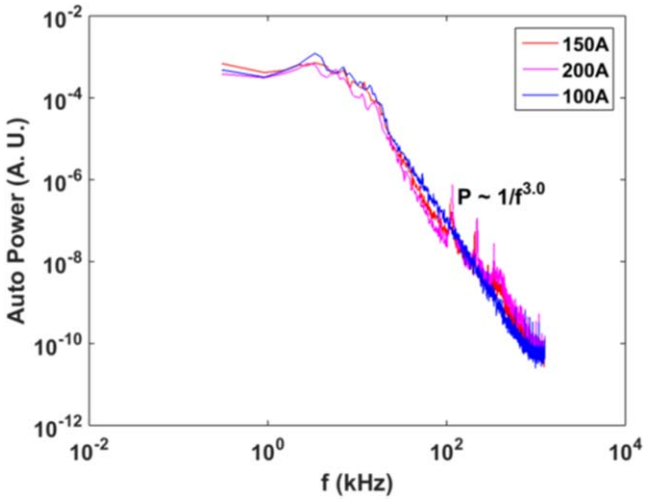

Figure 16. Auto-power spectrum of density fluctuation at $R = 0$ cm when core material is magnetized with different magnet current (I_{mag}).

measurements are carried out using two simple Langmuir probes of dimension 5 mm length and 0.5 mm diameter of tungsten tip and distance between two Langmuir probes is 5 mm. The density fluctuation measured across 10 kΩ resistance and floating potential fluctuation measured across 5 MΩ resistance with sampling rate 5 MS s^{-1} and record length 1 M point using same CRO. The density fluctuation and floating potential fluctuation found to hold the relation $\delta n/n \approx eV_f/k_BT$, this observation confirms the drift wave turbulence. But the power spectra of density fluctuation follow the power law $1/f^{3.0}$ as shown in figure 16 which is in contradiction with the power law of $1/f^{5.0}$ obtained by Chen *et al* for drift wave turbulence [27], to get the insight of this different observation of power law, we look back at the origin of the their argument. They have shown the dimensional arguments in deriving the K^{-5} wave spectra, this analogy do apply for the wave lengths (λ) of the perturbation in the range $L > \lambda > l_i$, where L is a length of the linear size of plasma and l_i is ion gyroradius. But in our case the wave lengths (λ) is much smaller than the ion gyroradius, as we are talking the phenomenon in null region The transition from f^{-5} to f^{-3} in the power law of density fluctuation has also been observed by D'Angelo *et al* in Q-machine [28]. Although we observed the power spectra which follows the power law f^{-5} where ions are magnetized and wave length of perturbation is much larger than the ion gyroradius [29].

5. Conclusion

A simulation of versatile multi-pole line cusp magnetic field (over a 1 m axial length and 40 cm diameter of the chamber) in vacuum is demonstrated using FEMM simulation tool. The magnetic field simulation results show generated VMMF has full control over a nearly field free region (null region) without changing poles of magnets and the rate of change of pole magnetic field with respect to magnet current is very high for vacoflux-50 core compared to simple air core. The argon plasma has been characterized in MMF. The experimental result shows the cusp magnetic field confines the primary electron at the center of the device. The confinement of plasma parameter (primary electron, plasma density and particle confinement time) improved with increasing magnetic field because of plasma leak width (leak rate) decreased thus stability of plasma increased with the magnetic field. The cusp magnetic field also filters the confined primary electrons across the magnetic field and the filtering strength of primary electrons across the magnetic field is increased with the magnetic field. Moreover the drift wave turbulence nature has been identified in a quiescent argon plasma confined at low magnetic field region of MMF. The control over the null region of MMF, mean plasma density, radial uniformity of plasma density with changing magnetic field and without changing the number of the poles of magnets are may be useful for new generation particle accelerator, plasma sources as well as NBI system of Tokomak in future.

ORCID iDs

M Sharma https://orcid.org/0000-0002-1745-6341

References

[1] Limpaecher R and MacKenzie K R 1973 *Rev. Sci. Instrum.* **44** 726
[2] Forest C *et al* 2015 *J. Plasma Phys.* **81** 345810501
[3] Karouta Fouad 2014 *J. Phys. D: Appl. Phys.* **47** 233501
[4] Günzel R, Wieser E, Richter E and Steffen J 1994 *J. Vac. Sci. Technol.* B **12** 927
[5] Lieberman M A and Lichtenberg A J 1994 *Principles of Plasma Discharges and Material Processing* (New York: Wiley-Interscience) 9780471724254 (https://doi.org/10.1002/0471724254)
[6] Mukherjee S and John P I 1997 *Surf. Coat. Technol.* **93** 188

[7] Grishm L R *et al* 2012 *Fusion Eng. Des.* **87** 1805
[8] Hosseinzadeh M and Afarideh H 2014 *Nucl. Instrum. Methods* A **735** 416
[9] Kim J H 2015 *Phys. Procedia* **66** 498
[10] Bosch R A and Merlino R L 1986 *Phys. Fluids* **29** 1998
[11] Bosch R A and Gilgenbach R M 1988 *Phys. Lett.* A **128** 437
[12] Herkowitz N, Leung K N and MacKenzie K R 1976 *Phys. Fluids* **19** 1045
[13] Jones R 1982 *Lett. Nuovo Cimento* **34** 157
[14] Kozima H, Kawamoto S and Yamagiwa K 1981 *Phys. Lett.* **86** 373
[15] Jones R 1979 *Plasma Phys.* **21** 505
[16] Jones R 1981 *Plasma Phys.* **23** 381
[17] Herkowitz N, Smith J R and Kozima H 1979 *Phys. Fluids* **22** 122
[18] Herkowitz N, Leung K N and Romesserg T 1975 *Phys. Lett.* **35** 227
[19] Hubble1 A, Barnat E V, Weatherford B R and Foster J E 2014 *Plasma Sources Sci. Technol.* **23** 022001
[20] Ault E R and MacKenzie K R 1973 *Rev. Sci. Instrum.* **44** 1697
[21] Meeker D 2015 Finite element method magnetics, Version 4.2, Users Manual http://www.femm.info
[22] Patel A D, Sharma M, Ramasubramanian N, Ganesh R and Chattopadhyay P K 2018 *Rev. Sci. Instrum.* **89** 043510
[23] Sheehan J P, Raitses Y, Hershkowitz N, Kaganovich I and Fisch N J 2011 *Phys. Plasmas* **18** 073501
[24] Bose S, Kaur M, Chattopadyay P K, Ghosh J, Saxena Y C and Pal R 2017 *J. Plasma Phys.* **83** 615830201
[25] Hershkowitz N, Leung K N and Romesser T 1975 *Phys. Rev. Lett.* **35** 277
[26] Aihara S, Fujiwara M, Hosokawa M and Ikegami H 1972 *Nucl. Fusion* **12** 45
[27] Chen F F 1965 *Phys. Rev. Lett.* **15** 381
[28] DÁngelo N, Pecseli H L and Peterson P I 1974 *Phys. Fluid* **17** 1853
[29] Patel A D, Sharma M, Ganesh R, Ramasubramanian N and Chattopadhyay P K 2018 *Phys. Plasmas* **25** 112114